Thermoelectric Properties of Sub-stoichiometric Electron Beam Patterned Bismuth Sulfide

Jose Recatala-Gomez,[1,2] Hong Kuan Ng,[1,3] Pawan Kumar,[1] Ady Suwardi,[1] Minrui Zheng,[4] Mohamed Asbahi,[1] Sudhiranjan Tripathy,[1] Iris Nandhakumar,[2*] Mohammad S. M. Saifullah[1*] and Kedar Hippalgaonkar[1,5*]

[1] Institute of Materials Research and Engineering, Agency for Science, Technology and Research (A*STAR), 2 Fusionopolis Way, Singapore 138634, Republic of Singapore

[2] Department of Chemistry, University of Southampton, University Road, Highfield, Southampton SO17 1BJ, United Kingdom

[3] Department of Physics, Faculty of Science, National University of Singapore, 2 Science Drive 3, Singapore 117551, Republic of Singapore

[4] Department of Electrical and Computer Engineering, Faculty of Engineering, National University of Singapore, 4 Engineering Drive 3, Singapore 117583, Republic of Singapore

[5] School of Material Science and Engineering, Nanyang Technological University, Block N4.1, 50 Nanyang Avenue, Singapore 639798, Republic of Singapore

KEYWORDS: thermoelectric, electron beam lithography, tellurium-free, thin film, sulfur vacancy, xanthate, bismuth sulfide

ABSTRACT

Direct patterning of thermoelectric metal chalcogenides can be challenging and is normally constrained to certain geometries and sizes. Here we report the synthesis, characterization, and direct writing of sub-10 nm wide bismuth sulfide (Bi_2S_3) using a single source, spin coatable, and electron beam sensitive bismuth(III) ethylxanthate precursor. In order to increase the intrinsically low carrier concentration of pristine Bi_2S_3, we developed a self-doping methodology in which sulfur vacancies are manipulated by tuning the temperature during vacuum annealing, to produce an electron-rich thermoelectric material. We report a room temperature electrical conductivity of 6 S m^{-1} and a Seebeck coefficient of -21.41 µV K^{-1} for a directly patterned, sub-stoichiometric Bi_2S_3 thin film. We expect that our demonstration of directly-writable thermoelectric films, with further optimization of structure and morphology can be useful for on-chip applications.

INTRODUCTION

The ever-increasing global energy consumption requires sustainable sources of electricity in order to meet the market's demand as well as to mitigate the effect of man-made climate change. Thermoelectric generators (TEG), which can directly convert heat to electricity, can effectively increase the sustainability of electricity production through the scavenging of waste heat.[1,2] Most work on TEGs has focused on bulk samples (either two-legged or single-leg devices), used in power generation from heat sources such as engines, power plants, and solar concentrators.[3–5] However, these devices cannot provide power generation in upcoming applications such as lab-on-a-chip devices,[6,7] biomedical devices[8] or wireless sensors for the Internet of Things.[9] Therefore, it would be of interest to develop high performance, and inexpensive materials whose fabrication can be cost-effective.[10,11] The performance of a TEG is related to the efficiency of the thermoelectric (TE) material which in turn is directly proportional to its dimensionless figure-of-merit (zT). zT is defined as $zT = (S^2\sigma T)/\kappa$, where S is the Seebeck coefficient, σ is the electrical conductivity, κ is the thermal conductivity, and T is the absolute temperature. Thus, in order to achieve high performance, a synergistic optimization of the carrier concentration is required.[2] The best material for room temperature applications is bismuth telluride (Bi_2Te_3) and its alloys, in both bulk and thin film forms.[12–14] However, tellurium's scarcity in the Earth's crust as well as its toxicity has motivated scientists to find cheaper, and non-toxic alternatives.[15–17] Sulfur (S), however, is abundant, inexpensive, and non-toxic. Therefore, bismuth sulfide (Bi_2S_3) could pose a good alternative to Bi_2Te_3 for room temperature TE applications. Biswas *et al.* reported that bulk Bi_2S_3 has a low electrical conductivity (≈ 4 S/cm at room temperature) due to the intrinsically low carrier concentration (3.7×10^{16} cm^{-3}) but a large Seebeck coefficient (-352 μW/K). This would result in poor performance, and therefore, the carrier concentration needs to be appropriately tuned.

One possibility of increasing the electrical conductivity is by self-doping *via* introducing sulfur vacancies in the crystal structure, resulting in an increase in the carrier concentration, since sulfur vacancies would act as electron donors.[18,19] Indeed, this was demonstrated by Zhao *et al.* in bulk Bi_2S_3 polycrystals, achieving a maximum *z*T of 0.11 at 523 K, and a twofold increase in the power factor ($S^2\sigma$) from 0.91 μW/cm K^2 for the pristine sample to 1.80 μW/cm K^2 in the sulfur-deficient sample (thereby called sub-stoichiometric).[20] Therefore, an ability to generate Bi_2S_3 in a form that is compatible with on-chip technologies is desirable. Amongst the top down fabrication techniques, electron beam lithography (EBL) is remarkable due to its high resolution and diversity of writable geometries, thus making it suitable for micro-TEG applications.[21] However, to overcome the problems arising during the lift-off step traditionally utilized in organic resists during conventional EBL, we employed metalorganic resists that do not require (or require very little) chemical development.[22] These resists have been developed for direct patterning of metal oxides (ZnO)[23] and metal sulfides such as ZnS[24] and MoS_2[25] albeit not for thermoelectric materials. In this work, we present a top-down approach for the synthesis of thermoelectric Bi_2S_3, leveraging upon the versatility of electron beam lithography combined with the advantages of metalorganic resists. We synthesized bismuth(III) ethylxanthate, a single source precursor and demonstrated the nanoscale patterning of pristine Bi_2S_3 comprised of sub-10 nm grid lines and micron-sized thin films. Moreover, we developed a methodology to self-dope the patterned films, introducing sulfur vacancies, and thus increasing the electron concentration, thereby realizing the first *n*-type directly writable thermoelectric material that is potentially compatible with micro-TEG for on-chip applications.

RESULTS AND DISCUSSION

Bismuth(III) ethylxanthate, a yellow powder, was synthesized from a one-to-three molar mixture of bismuth(III) nitrate and potassium ethylxanthate in an aqueous medium. The thermal characteristics of the powder were evaluated by means of thermogravimetric analysis (TGA) and differential scanning calorimetry (DSC) as shown in Figure 1(a). The TGA curve shows a steep one-step mass loss, starting at ~110 °C, until 161 °C, and subsequently a stable behavior with no reduction in mass is seen. The material decomposed to 45.8% of its original mass at 161 °C. This corresponds very well with the theoretical value of 44.7% for Bi_2S_3 obtained using calculations. Close correspondence between the obtained and theoretical mass losses suggests that the end product is most likely Bi_2S_3 and has a fairly high purity. The DSC analysis shows the melting of bismuth(III) ethylxanthate at ~110 °C with simultaneous decomposition. A smaller endotherm is observed later at about 160 °C, most likely due to atomic rearrangement leading to crystallization of the material. No further heat changes were observed when heated to 500 °C. The formation of pristine Bi_2S_3 is confirmed by means of x-ray diffraction (XRD). Figure 1(b) shows the diffractogram of bismuth(III) ethylxanthate film heat-treated at 350 °C for 30 minutes [inset in Figure 1(b)]. All the observed peaks are in good agreement with JCPDS card 01-074-9437 thus confirming the formation of Bi_2S_3.[26] Details of morphology and elemental composition can be found in Supporting Information Figure S2.

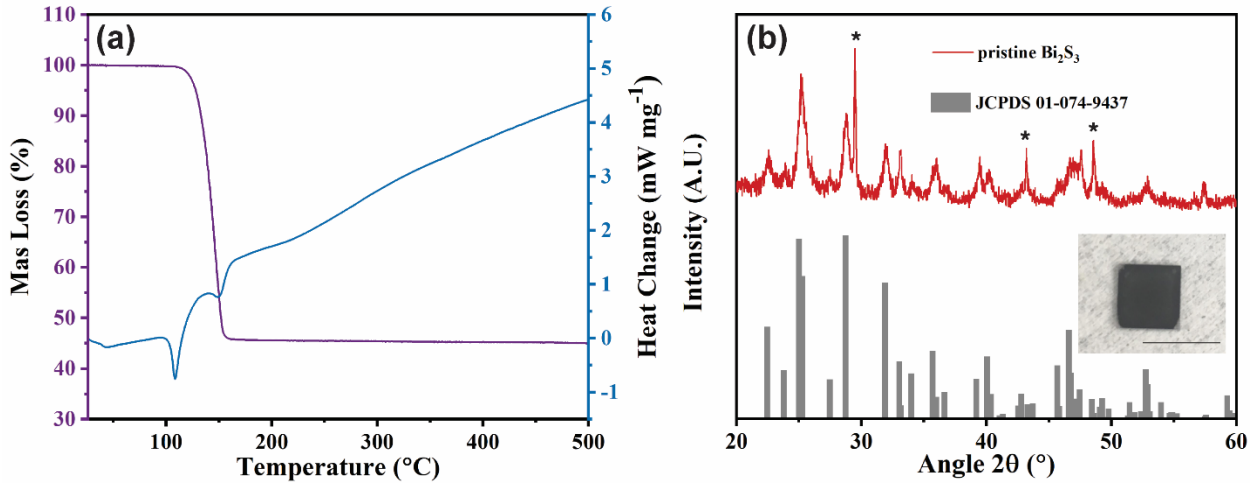

Figure 1. (a) TGA and DSC data of bismuth(III) ethylxanthate. (b) XRD pattern of as-deposited film (red) and the matching JCPDS card 01-074-9437 (grey), showing the formation of Bi_2S_3. The peak marked with an asterisk (*) corresponds to the quartz substrate. Inset shows an optical image of a heat-treated sample on a 7 × 7 mm quartz substrate (scale bar = 10 mm).

The electron beam exposure response behavior of bismuth(III) ethylxanthate resist [Figure 2(a)] was studied by exposing pre-defined lines (Supporting Information Figure S3) at various doses. The heights of these lines were measured using an atomic force microscope (AFM), and their normalized values were plotted against the dose [Figure 2(b)]. From this plot, two crucial parameters were extracted – sensitivity and contrast.[27] Sensitivity is a parameter that quantifies the minimum amount of delivered dose that is required to achieve the selective development (in other words, how impactful is the electron beam dose on the resist). The contrast (γ), whose mathematical description for a negative tone resist is $\gamma = \log (D_{100}/D_0)^{-1}$, where D_{100} and D_0 are the minimum dose at which the resist has undergone a complete change of its chemical structure and the highest dose at which the resist is not yet affected by electron irradiation, respectively, describes how easy it is to differentiate between exposed and unexposed areas of the resist.[22] The

sensitivity of bismuth(III) ethylxanthate was found to be 5.4 mC/cm^2. This value is much lower than the sensitivity values reported for other negative chalcogenide resists such as ZnS and MoS_2 resists (~35 mC/cm^2).[24,25] In order to understand the effect of electron dose on bismuth(III) ethylxanthate, circular discs of 50 µm were patterned using an electron beam to perform micro-FTIR and micro-Raman spectroscopies [Figures 2(c) and 2(d), respectively]. Micro-FTIR spectroscopy results suggest that the exposure to a beam of electrons leads to the disappearance of xanthate moieties represented by ν(C=S) at 1044 cm^{-1} and ν(C–O) at 1121 cm^{-1} most likely *via* the Chugaev elimination [Figure 2(c)].[28,29] A broad unidentified peak centred at 972 cm^{-1} appears. Analysis of the same using micro-Raman spectroscopy [Figure 2(d)] shows the appearance of characteristic peaks of Bi_2S_3 at 232, 256, 307, and 428 cm^{-1}.[30–32] In other words, the organic parts in bismuth(III) ethylxanthate, *i.e.*, the xanthate moieties, decompose under an electron beam leaving behind Bi_2S_3. Appearance of Bi_2S_3 makes the exposed resist insoluble in organic solvents such as *iso*-propyl alcohol. This property was utilized to pattern nanoscale Bi_2S_3 lines. Figures 2(e) and 2(f) show 9 nm wide lines in a grid of pitch 100 nm. Our technique offers the ability to pattern diverse shaped structures with the potential for precisely positioning them in any area of a substrate. Taking a cue from an earlier study on UV and EUV exposure of copper and indium xanthates to produce their respective metal sulfides, we surmise that bismuth(III) ethylxanthate can also be patterned using UV radiation to produce Bi_2S_3.[33]

Once the properties of the resist have been assessed over a wide range of dose and annealing conditions and the optimal parameters for patterning are determined (Supporting Information Figures S4 and S5), we proceeded to study the electrical properties of pristine Bi_2S_3. Bismuth(III) ethylxanthate was drop casted on a 7 × 7 mm^2 quartz substrate and annealed at 350 °C for 30 minutes. Both drop casting and annealing were conducted inside a glove box to prevent oxidation.

The electrical properties of as-deposited films were measured, and the resistance was found to ~1 MΩ (Supporting Information Figure S6). This indicates a low carrier concentration, as expected based on previous studies on bulk pristine Bi_2S_3.[34]

Next, we conducted annealing at various temperatures in vacuum (pressure ~ 10^{-2} Torr) in order to create sulfur (S) vacancies and increase the carrier concentration.[20] Experiments were carried out in steps of 25 °C, at 400 °C, 375 °C, 350 °C, and 300 °C with a heat-treatment time of 2 hours at each temperature. The impact of vacancy introduction on the crystal structure was investigated by means of XRD. The diffractogram for the film annealed at 400 °C resulted in a Bi-rich phase [Supporting Information, Figure S7(a)]. For annealing temperatures below 400 °C [Figure 3(a)], all peaks were indexed to the diffraction peaks of JCPDS card 01-074-9437, just as in the pristine case [Figure 1(b)].[26] The two low intensity peaks [marked with an asterisk in Figure 3(a)] were found to match a mixed Bi-O-S sub-oxide (JCPDS card 01-084-7195).[35]

The formation of S vacancies and their quantification was determined by x-ray photoelectron spectroscopy (XPS). Figure 3(b) and Supporting Information Figure S1 show the core levels of Bi 4f and S 2s, respectively, of a film vacuum-annealed at 350 °C. The peaks in Figure 3(b) are centred at 158.51 eV and 163.83 eV and the peak at binding energy of 225.60 eV in Supporting Information Figure S1 confirms the formation of Bi_2S_3.[36] The weak intensity of the peaks corresponding to Bi_2O_3 in comparison to the peaks corresponding to Bi_2S_3 in Figure 3(b) may imply that Bi_2O_3 only appears as a thin layer on the surface of the sample and does not appear as a phase throughout the thickness of the film. The peak centered at 157.59 eV in Figure 3(b) corresponds to uncoordinated Bi, thereby confirming the existence of sulfur vacancies in the films.[36,37,38] The atomic ratio of Bi to S was calculated from the areas of Bi $4f_{7/2}$ and S $2p_{3/2}$ and the results are summarized in Figure 3(c).

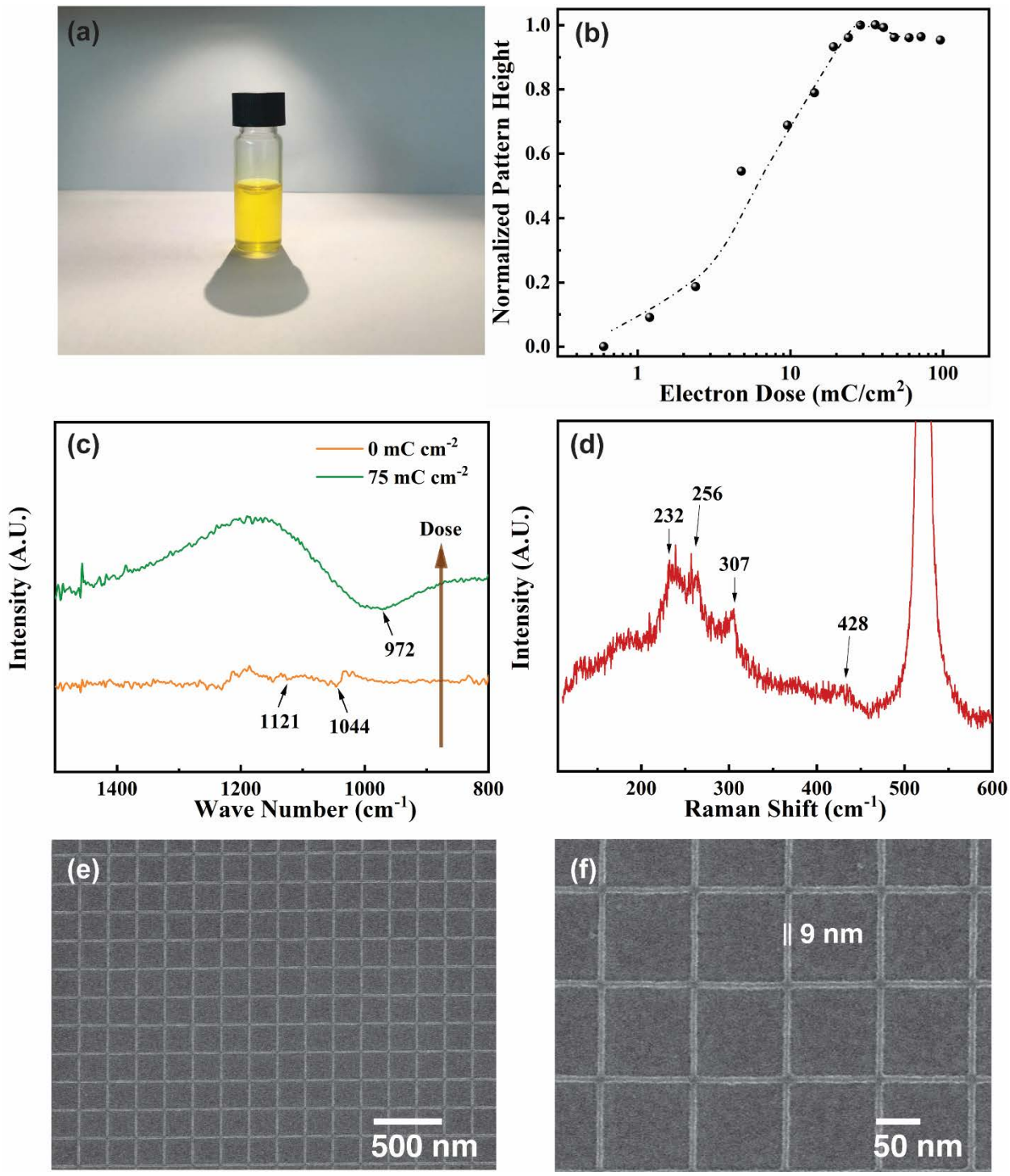

Figure 2. (a) Optical image of the prepared Bi_2S_3 resist used for electron beam patterning. (b) Electron beam sensitivity curve for bismuth(III) ethylxanthate. (c) Micro-FTIR and (d) micro-Raman study of electron beam exposed bismuth(III) ethylxanthate resist showing the appearance of Bi_2S_3 peaks. (e) Scanning electron

micrograph of a directly written grid with 9 nm Bi_2S_3 lines, and (f) magnified image of the same. For fine patterning, the substrates were 1 cm × 2 cm silicon wafers with 50 nm thick CVD-grown Si_3N_4 on top.

The electrical conductivity of the vacuum annealed samples was measured, and the room temperature values are plotted in Figure 3(c). We concluded that 300 °C was the minimum vacuum annealing temperature necessary to introduce S vacancies that contributed to the total carrier concentration in this system and that 400 °C is the upper boundary in the temperature scale for operation, since the films become mechanically unstable with all sulfur removed according to the XPS analysis [see Supporting Information, Figures S7(c) and (d)]. We observed a monotonic increase in conductivity with annealing temperature, indicating that charge carriers were being created as sulfur was removed, peaking at 375 °C. The manipulation of charge carriers by tuning the annealing temperature was further verified by the change in Seebeck coefficient of the films with sulfur removal, shown in Figure 3(d). According to the Mott formula, $S \propto \left(\frac{1}{n}\right)^{2/3}$ and therefore an increase in carrier concentration will be accompanied by a decrease in Seebeck coefficient.[2] This trend is observed in our case, as well as observed by Zhao *et al.* for bulk polycrystalline samples.[20] Attempts to measure the Seebeck coefficient of the film annealed at 375 °C were unsuccessful due to difficulties in generating a sufficient temperature gradient. This temperature also provokes a certain degree of delamination of the films. Hence, the second best condition, annealing at 350 °C was used for further experiments, as it is the best compromise between enhancement in electrical conductivity and mechanical stability.

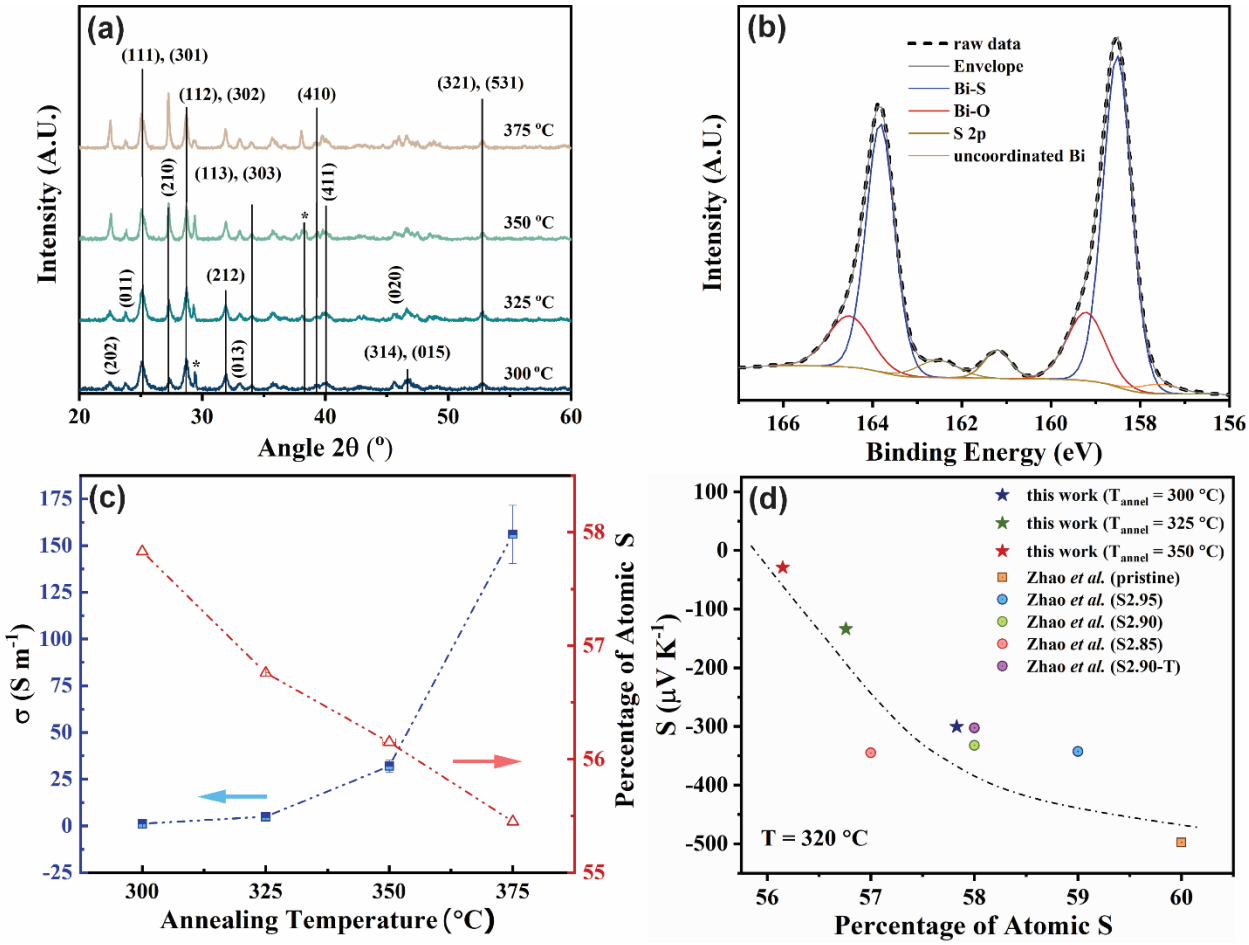

Figure 3. (a) XRD diffraction patterns of sub-stoichiometric Bi_2S_3 annealed in vacuum at different temperatures. (b) XPS core level spectra of Bi 4f. The presence of a peak corresponding to uncoordinated Bi indicates that S has been removed during the treatment, effectively creating S vacancies that act as electron donors. Also shown is S 2s spectrum from the film annealed at 350 °C. (c) Room temperature electrical conductivity (σ) and percentage of atomic S present in the film as a function of the annealing temperature in vacuum. (d) Seebeck coefficient *versus* percentage of atomic sulfur. The literature points correspond to data from Zhao *et al.*[20] The black, discontinuous line is a guide to the eye.

We now proceed to study the electrical properties of directly patterned thin films of Bi_2S_3. These were prepared by electron beam exposure of the resist and subsequently heat-treated at 350 °C for

30 minutes in a glovebox before transferring them to a vacuum furnace for thermal annealing at the same temperature. Figure 4(a) shows a top view SEM image of a directly written sub-stoichiometric Bi_2S_3 thin film, annealed at 350 °C for 2 hours. The film has lower packing density, and therefore, lower electrical conductivity should be expected, since the electron mobility would be reduced. In order to gain better insights into the topography of the film, atomic force microscopy (AFM) measurements were carried out and the results are shown in Figure 4(b) and Supporting Information Figure S9. Five different profiles were taken, revealing an average thickness of 14.7 ± 0.54 nm. In addition, five profiles across the film were also taken and the root mean square (RMS) roughness was found to be 1.26 ± 0.11 nm. Since the film was very thin, the sheet resistance was expected to be high. The lower thickness and higher RMS roughness in comparison to the pristine film (0.65 ± 0.08 nm, Supporting Information Figure S10) indicates that the thermal treatment has a direct impact on increasing its roughness. Also, there are nanopores distributed throughout the surface of the film, with an average pore size of 73.11 ± 23.67 nm. Porosity could reduce the lattice thermal conductivity, as demonstrated by Shi *et al.* in bulk polycrystalline tin selenide (SnSe). They achieved selective porosity by decomposing a host material (indium selenide nanoprecipitates, InSe) into the SnSe matrix during sintering, which resulted in a lower thermal conductivity.[39] Furthermore, although our resist is capable of sub-10 nm resolution, observing porosity after vacuum annealing implies that its patterning at that scale has limited usefulness due to difficulty in electrical measurements.

A device for the simultaneous measurement of the in-plane thermoelectric properties (Seebeck coefficient and electrical conductivity)[40] was patterned by means of electron beam lithography [Figure 4(c)]. When measured using a room temperature four-point probe, the sheet resistance drops to 570 kΩ for the directly written film vacuum-annealed at 350 °C for 2 hours [Supporting

196 Information Figure S12(b)]. Figure 4(d) shows the temperature-dependent electrical conductivity
197 and Seebeck coefficient of a typical patterned film annealed at 350 °C in vacuum. Despite the
198 presence of nanopores, 100% relative density has been considered when measuring the electrical
199 conductivity, as this represents the lower bound for electrical conductivity values. The electrical
200 conductivity at room temperature was found to be 6 S m^{-1}, which is higher than reports for other
201 chemically grown films via chemical deposition [41,42] and dip-coating[43] as well as previous reports
202 for physically grown films using thermal evaporation[44], which typically report an electrical
203 conductivity only as large as 0.1 S m^{-1}. Hence, our values are 60 times higher due to the novel
204 solution-processable and post-processing techniques, in addition to having the potential to be
205 compatible to on-chip technologies at the nanoscale. However, these values are small in
206 comparison with their bulk counterparts, and is attributed to the smaller grain size of chemically
207 deposited bismuth sulfide in comparison with sintered powders.[20]. The strategies deployed for
208 chemical thin film growth are not compatible with on-chip technologies, in addition of being rather
209 cumbersome processes. On the other hand, our method offers a reasonably quick and an
210 inexpensive alternative, that can be performed in a high throughput fashion.[45] Finally, from the
211 temperature-dependent electrical conductivity, an Arrhenius fit [$\sigma = A \exp(-E_a/k_BT)$, where A is a
212 prefactor, k_B is the Boltzmann constant and T is the absolute temperature] was performed for a
213 single carrier activation energy (E_a), calculated from the slope of the $\ln(\sigma)$ *versus* T^{-1} and was
214 found to be ~80 meV. This is the energy required for the trapped defect states to become free
215 charge carriers that will contribute to the overall carrier concentration. Interestingly, the Seebeck
216 coefficient is smaller (-20.68 µV K^{-1} at 323 K) than the Seebeck coefficient reported for a bulk
217 polycrystalline sample at the same temperature, indicating that the carrier concentration is past the
218 optimal point. The closeness of the Seebeck coefficient of patterned film and the Seebeck

coefficient of its drop-casted counterpart (-29.37 μV K^{-1}) indicate that the nominal carrier concentration is in a similar range and therefore the difference in electrical conductivity between the two comes from the difference in mobilities. Attempts at measuring the Hall coefficient, despite the patterning of Hall electrodes, proved futile due to the low electrical conductivity and large porosity of the films. The carrier concentration (n) was calculated by solving the linearized Boltzmann Transport Equation at 325 K and $m_{DOS} = 0.333m_e$[46] and it was found to be 1.03×10^{20} cm^{-3}, which is higher than the carrier concentrations reported by Zhao *et al.* (largest $n = 4.17 \times 10^{18}$ cm^{-3}).[20] Using the relationship $\sigma = ne\mu$ (where μ is the mobility, σ is the electrical conductivity, e is the electron charge and n is the carrier concentration), the mobility at this doping level was calculated to be 4.91×10^{-3} cm^2 V^{-2} s^{-1}. This value is substantially smaller in comparison to the values reported by Zhao *et al.* (Supporting Figure S13).[20] This could be attributed to the lower carrier concentration reported in their work (two orders of magnitude lower than the carrier concentration reported herein and hence a larger mobility) and especially to the dissimilar synthesis and post-processing conditions. Zhao *et al.* sintered the samples, which led to larger grain sizes (in the order of microns) whilst in our case, the grain size is in the order of tens of nanometers. Hence, charge carriers will suffer more scattering events in nanocrystalline samples rather than in sintered ones. In order to improve the mobility, larger grains could be realized in our samples by adding another step to the post-processing workflow: after vacuum annealing, one could perform light sintering, locally melting parts of the film and therefore allowing it to recrystallize and form larger grains.[47] This will increase the mobility for a fixed carrier concentration, therefore increasing the electrical conductivity.

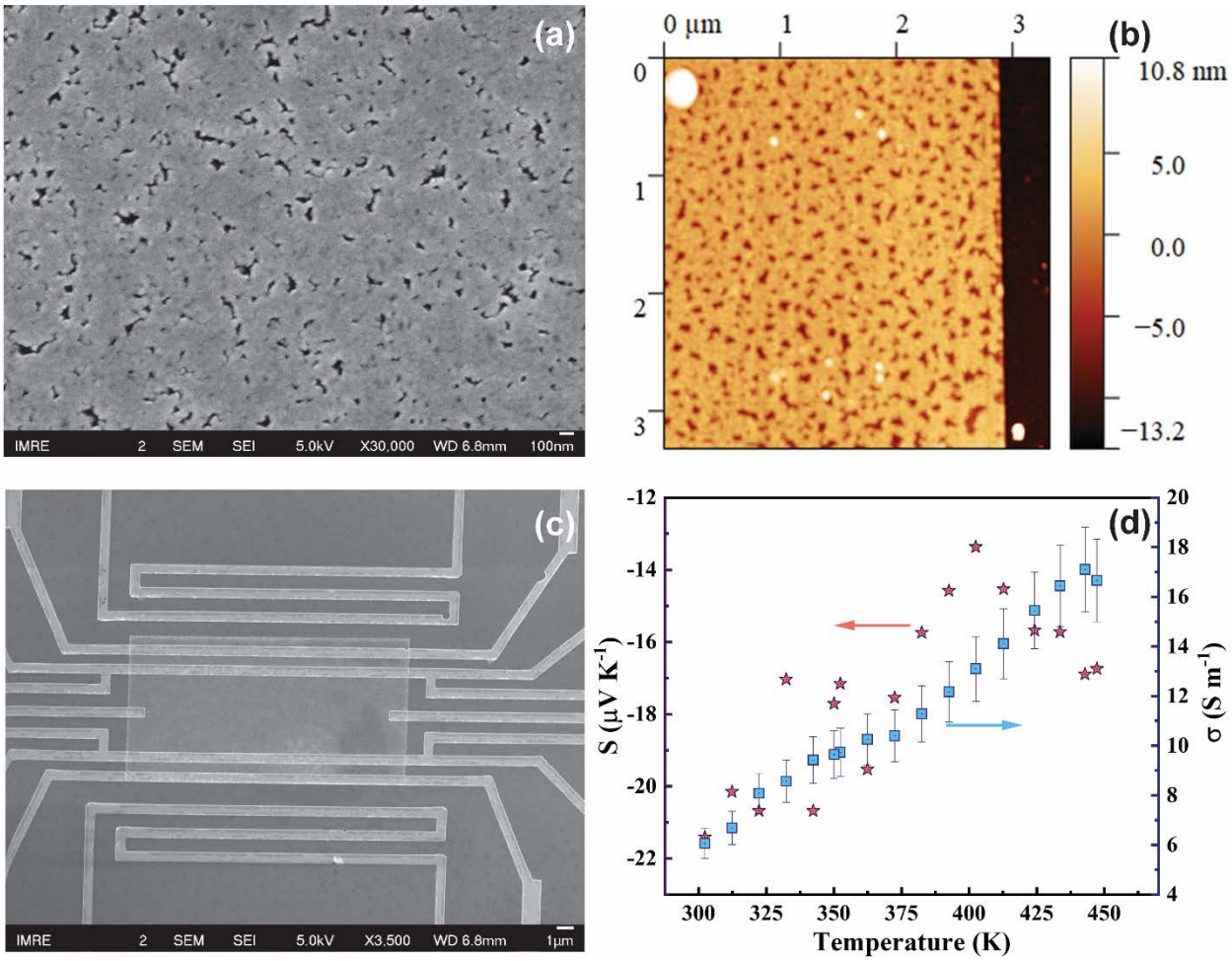

Figure 4. (a) Top view SEM and (b) AFM tapping mode image of a directly written film, annealed under vacuum at 350 °C for 2 hours. (c) Device for TE measurements. (d) Temperature-dependent Seebeck coefficient and electrical conductivity for this film. The 10% error bars in the measured electrical conductivity are commensurate with the observed porosity in the films from Figure 4(c) and will result in an underestimate of the actual electrical conductivity.

241

242 **CONCLUSIONS**

243 A framework for the direct nanoscale patterning of arbitrarily shaped bismuth sulfide (Bi_2S_3) *via*
244 electron beam lithography has been developed. A self-doping strategy was deployed in order to
245 increase the inherently low carrier concentration of pristine Bi_2S_3, achieved by selectively

introducing S vacancies in the films during vacuum annealing at temperatures ranging from 300 °C to 400 °C. XRD measurements confirm that the structure remains unchanged until 400 °C whilst XPS measurements demonstrate that as the annealing temperature increases, the atomic percentage of sulfur decreases, accompanied by the presence of a peak centered at binding energy of 157.59 eV, corresponding to uncoordinated Bi species. The correlation between sulfur vacancies and electroactive charge carriers is further confirmed by electrical and Seebeck measurements, which show an increase of the electrical conductivity with corresponding decrease in sulfur content, as well as a decrease in Seebeck coefficient with decreasing sulfur content, as predicted by the Mott formula. We determined that annealing at 350 °C in mild vacuum (10^{-2} Torr) for two hours is the optimal post-processing condition for sulfur vacancy introduction and film adherence to the substrate. Therefore, a thin film was patterned, post-treated, and its temperature-dependent thermoelectric properties evaluated. We report a low electrical conductivity (σ) of 6 S m^{-1} at room temperature. SEM and AFM studies show that the films have nanoporous structures; responsible for low mobility, and in turn, leading to a low electrical conductivity. The room temperature Seebeck coefficient of -21.41 μV K^{-1} indicates that the carrier concentration is past the optimum point, in line with the theoretical calculation of carrier concentration using Boltzmann Transport Equations. An enhancement in the electrical properties could be achieved by improving the post-processing, in order to increase the average grain size and therefore increase the mobility. The lattice thermal conductivity could also be decreased by manipulating the porous nanostructures to act as phonon scattering centers. These two strategies may potentially result in an overall enhancement of the figure-of-merit (zT). In addition, the development of a *p*-type inorganic, electron sensitive resist is necessary in order to realize a fully functioning TEG that provides power generation when coupled to an on-chip microdevice.

Materials and Methods

Reagents

Bismuth nitrate (99.99%), hydrochloric acid (37%), anisole (anhydrous, 99.7%) and chloroform (≥99.5%) were purchased from Sigma-Aldrich (Singapore). Potassium ethylxanthate (96%) was purchased from TCI Chemicals, Japan. All reagents were used without further purification.

Synthesis of the Resist

The two step synthesis was done by dissolving 2.0 g of powder bismuth nitrate, $Bi(NO_3)_3$, in 50.0 mL deionized water, with the consequent formation of a white precipitate of $Bi(OH)_3$. Next, hydrochloric acid (HCl) was added dropwise with vigorous stirring in order to dissolve this precipitate and form $BiCl_3$. The reactions proceed as follows:

$$Bi(NO_3)_3 + 3H_2O \rightarrow Bi(OH)_3 + 3HNO_3$$

$$Bi(OH)_3 + 3HCl \rightarrow BiCl_3 + 3H_2O$$

A slight excess of potassium ethylxanthate, 2.05 g, was dissolved into 50.0 mL deionized water, forming a clear yellow solution. It was added slowly to the first solution with vigorous stirring which reacted immediately to form yellow precipitate of bismuth(III) ethylxanthate ($C_9H_{15}BiO_3S_6$). The solution is let to stir for another 30 minutes to ensure the completion of reaction. The resulting mixture was filtered, and the precipitate rinsed with deionized water thrice and put under a fumehood overnight for drying. This was followed by 24 hours of drying in a

vacuum oven. At the end, 2.5 g of bismuth ethylxanthate, a bright yellow powder, was obtained after drying (yield = 82.6%).

Directly Written Thin Film and Device Fabrication

For thermoelectric measurements, the substrates used were 2 × 2 cm segments of *p*-type Si (100) with 300 nm of SiO_2 on top. They were sonicated for 5 minutes in deionized water, acetone, and *iso*-propyl alcohol and treated with ozone for 10 minutes at 100 °C. For fine patterning, the substrates were 1 cm × 2 cm silicon wafers with 50 nm thick CVD-grown Si_3N_4 on top. Bi_2S_3 resist was prepared by adding 30 mg of bismuth(III) ethylxanthate in 0.5 mL of chloroform and then add 0.5 mL anisole to it. All the resist solutions were filtered before spin-coating by means of a syringe filter. The samples for electron beam patterning were prepared by spin-coating 100 µL of a solution. Electron beam patterning was conducted using an Elionix ELS 7000 electron beam lithography machine operating at 100 kV with a probe current of 0.8 nA. The exposed resist was developed and rinsed in *iso*-propyl alcohol for 30 s each.

The device for TE measurements was fabricated using a multistep standard nanofabrication procedure, involving coating of poly(methyl methacrylate) (PMMA) resist, and electron beam lithography, metal deposition (10 nm Ti and 100 nm Au), and lift-off in acetone. The device consisted of two thermometers, two heaters, two Hall bars and four lines for resistivity measurement.[40]

Introduction of Sulfur Vacancies *via* Vacuum Annealing

Pristine Bi_2S_3 thin films are very resistive due to the intrinsically low conductivity of Bi_2S_3[34] and the small geometry and thickness of the patterned films. In order to decrease the resistance and therefore be able to measure the thermoelectric properties of the films, sulfur vacancies were induced. Owing to the low vapor pressure of sulfur, vacuum annealing under inert conditions at a temperature above the vaporization pressure can induce sulfur vacancies, in a mechanism that resembles the formation of oxygen vacancies in thermoelectric oxides, such as ZnO and $SrTiO_3$.[48–50] Annealing was conducted at different temperatures in order to manipulate the sulfur vacancy concentration in a tube furnace at a pressure below 10^{-2} Torr for 2 hours. Forming gas (4% H_2, 96% Ar) was continuously pumped into the furnace at 100 sccm in order to avoid oxygen contamination.

Material Characterization

Thermogravimetric analysis (TGA) and differential scanning calorimetry (DSC) were performed in a nitrogen atmosphere (flow rate = 30 mL/min; heating rate = 10 °C/ min) using a Netzsch STA 449 F1 Jupiter simultaneous thermal analyzer.

In order to have a large material area for characterization, thin films were fabricated by drop casting the resist on 7 × 7 mm segments of *p*-type Si (100) with 300 nm of SiO_2 on top, cleaned as described earlier. Both drop casting and subsequent annealing were carried out in a glovebox in order to avoid oxidation.

A JEOL JSM 7600F FEG-scanning electron microscopy (SEM) was utilized to investigate the morphology of both the directly-written and the drop-casted films.

The topography and thickness of the directly written thin films were evaluated using an atomic force microscopy (AFM). A SPM Brucker/Veeco DI 3100 AFM operating in tapping mode using

an undoped silicon cantilever with a force constant of 10-130 N/m was purchased from Nanosensors™. The acquired AFM images were processed using the Nanoscope Analysis 1.10 software.

X-ray diffraction (XRD) was used to investigate the crystal structure and crystalline phases of the drop casted samples. Measurements were conducted by means of a Bruker D8 Advance (x-ray source: Cu-K_α) and phase identification was conducted using Bruker's EVA software.

X-ray photoelectron spectroscopy (XPS) was employed for the elemental quantification as well as oxidation state identification of the heat-treated films. A Thermo Scientific Theta Probe XPS equipped with a monochromatic Al-K_α x-ray source (energy = 1486.7 eV) was used for spectra acquisition. The x-ray spot was adjusted to 400 μm in diameter with an x-ray incident angle fixed to 30° with respect to normal surface. Charge compensation was achieved using low energy electron flooding. Survey scans were acquired at step a 1 eV and pass energy of 200 eV whilst the narrow scans were acquired at step of 0.1 eV and pass energy of 40 eV. Data analysis was conducted using the Advantage software.

In-plane, temperature dependent Seebeck coefficient and electrical conductivity were simultaneously measured in a home-built cryostat under high vacuum ($\approx 5\times10^{-7}$ Torr). The samples were placed in a 24 pin chip carrier and electrical connection between the device contacts and the chip carrier were established by means of a West Bond wirebonder equipped with an aluminum thread. Details of the measurement can be found in Kumar *et. al.*[40]

ASSOCIATED CONTENT

Supporting Information

The Supporting Information is available free of charge on the ACS Publications website at DOI:

Figure S1: Material characterization of a bismuth(III) ethylxanthate film heat-treated at 350 °C for 30 minutes: SEM images [(a) and (b)] and elemental maps for bismuth [Bi, (c)] and sulfur [S, (d)]

Figure S2: AFM topography images of pre-defined lines exposed at different doses.

Figure S3: Optical images of bismuth(III) ethylxanthate thin films exposed at different doses.

Figure S4: Optical images of bismuth(III) ethylxanthate thin films annealed at different temperature and time.

Figure S5. Optical image of the device for thermoelectric measurements and room temperature four probe resistivity measurement of pristine Bi_2S_3.

Figure S6: Material characterization of a pristine Bi_2S_3 film annealed at 400 °C: XRD and XPS.

Figure S7: Optical images of a pristine Bi_2S_3 thin film before and after annealing at 400 °C.

Figure S8: Extended AFM data for the directly written thin film annealed at 350 °C.

Figure S9: Extended AFM data for the directly written pristine thin film.

Figure S10: EDX elemental mapping of a substoichiometric, directly patterned thin film.

Figure S11: Nanopatterned device for thermoelectric measurements and room temperature four-point probe I-V curve measured for a substoichiometric Bi_2S_3 thin film, annealed at 350 °C.

AUTHOR INFORMATION

Corresponding Author

*E-mail: kedar@ntu.edu.sg, saifullahm@imre.a-star.edu.sg , iris@soton.ac.uk

ORCID

Jose Recatalà-Gómez: 0000-0003-3560-2768

Ng Hong Kuan: 0000-0001-6781-5827

Pawan Kumar: 0000-0001-9772-5638

Ady Suwardi: 0000-0002-7342-0431

Zheng Minrui: 0000-0002-1245-3360

Mohamed Asbahi: 0000-0002-4442-6121

Sudhiranjan Tripathy:

Iris Nandhakumar: 0000-0002-9668-9126

M.S.M Saifullah: 0000-0002-3172-041X

Kedar Hippalgaonkar: 0000-0002-1270-9047

Author Contributions

The manuscript was written through contributions of all authors. All authors have given approval to the final version of the manuscript.

Acknowledgements

AS, PK and KH would like to acknowledge funding from the Accelerated Materials Development for Manufacturing Program at A*STAR via the AME Programmatic Fund by the Agency for Science, Technology and Research under Grant No. A1898b0043. JR-G and IN would like to thank A*STAR Graduate Academy's ARAP programme for funding JR-G's graduate studies in IMRE, A*STAR.

Notes

Any additional relevant notes should be placed here.

References

(1) Bell, L. E. Cooling, Heating, Generating Power, and Recovering Waste Heat with Thermoelectric Systems. *Science* **2008**, *321* (5895), 1457–1461. https://doi.org/10.1126/science.1158899.

(2) Snyder, G. J.; Toberer, E. S. Complex Thermoelectric Materials. *Nat. Mater.* **2008**, *7* (2), 105–114. https://doi.org/10.1038/nmat2090.

(3) Mao, J.; Zhu, H.; Ding, Z.; Liu, Z.; Gamage, G. A.; Chen, G.; Ren, Z. High Thermoelectric Cooling Performance of N-Type Mg3Bi2 -Based Materials. *Science (80-.).* **2019**, *365* (6452), 495–498. https://doi.org/10.1126/science.aax7792.

(4) Kraemer, D.; Poudel, B.; Feng, H.-P.; Caylor, J. C.; Yu, B.; Yan, X.; Ma, Y.; Wang, X.; Wang, D.; Muto, A.; McEnaney, K.; Chiesa, M.; Ren, Z.; Chen, G. High-Performance Flat-Panel Solar Thermoelectric Generators with High Thermal Concentration. *Nat. Mater.* **2011**, *10* (7), 532–538. https://doi.org/10.1038/nmat3013.

(5) Perumal, S.; Samanta, M.; Ghosh, T.; Shenoy, U. S.; Bohra, A. K.; Bhattacharya, S.; Singh, A.; Waghmare, U. V.; Biswas, K. Realization of High Thermoelectric Figure of Merit in GeTe by Complementary Co-Doping of Bi and In. *Joule* **2019**, *3* (10), 2565–2580. https://doi.org/10.1016/j.joule.2019.08.017.

(6) Chowdhury, I.; Prasher, R.; Lofgreen, K.; Chrysler, G.; Narasimhan, S.; Mahajan, R.; Koester, D.; Alley, R.; Venkatasubramanian, R. On-Chip Cooling by Superlattice-Based Thin-Film Thermoelectrics. *Nat. Nanotechnol.* **2009**, *4* (4), 235–238. https://doi.org/10.1038/nnano.2008.417.

(7) Hu, G.; Edwards, H.; Lee, M. Silicon Integrated Circuit Thermoelectric Generators with a High Specific Power Generation Capacity. *Nat. Electron.* **2019**, *2* (7), 300–306. https://doi.org/10.1038/s41928-019-0271-9.

(8) Sanders, G. H. W.; Manz, A. Chip-Based Microsystems for Genomic and Proteomic Analysis. *TrAC Trends Anal. Chem.* **2000**, *19* (6), 364–378. https://doi.org/10.1016/S0165-9936(00)00011-X.

(9) Rojas, J. P.; Singh, D.; Inayat, S. B.; Sevilla, G. A. T.; Fahad, H. M.; Hussain, M. M. Review—Micro and Nano-Engineering Enabled New Generation of Thermoelectric Generator Devices and Applications. *ECS J. Solid State Sci. Technol.* **2017**, *6* (3), N3036–N3044. https://doi.org/10.1149/2.0081703jss.

(10) Snyder, G. J.; Lim, J. R.; Huang, C.-K.; Fleurial, J.-P. Thermoelectric Microdevice Fabricated by a MEMS-like Electrochemical Process. *Nat. Mater.* **2003**, *2* (8), 528–531. https://doi.org/10.1038/nmat943.

(11) Li, G.; Garcia Fernandez, J.; Lara Ramos, D. A.; Barati, V.; Pérez, N.; Soldatov, I.; Reith, H.; Schierning, G.; Nielsch, K. Integrated Microthermoelectric Coolers with Rapid

Response Time and High Device Reliability. *Nat. Electron.* **2018**, *1* (10), 555–561. https://doi.org/10.1038/s41928-018-0148-3.

(12) Poudel, B.; Hao, Q.; Ma, Y.; Lan, Y.; Minnich, A.; Yu, B.; Yan, X.; Wang, D.; Muto, A.; Vashaee, D.; Chen, X.; Liu, J.; Dresselhaus, M. S.; Chen, G.; Ren, Z. High-Thermoelectric Performance of Nanostructured Bismuth Antimony Telluride Bulk Alloys. *Science* **2008**, *320* (5876), 634–638. https://doi.org/10.1126/science.1156446.

(13) Kim, S. I.; Lee, K. H.; Mun, H. A.; Kim, H. S.; Hwang, S. W.; Roh, J. W.; Yang, D. J.; Shin, W. H.; Li, X. S.; Lee, Y. H.; Snyder, G. J.; Kim, S. W. Dense Dislocation Arrays Embedded in Grain Boundaries for High-Performance Bulk Thermoelectrics. *Science (80-.).* **2015**, *348* (6230), 109–114. https://doi.org/10.1126/science.aaa4166.

(14) Venkatasubramanian, R.; Silvola, E.; Colpitts, T.; O'Quinn, B. Thin-Film Thermoelectric Devices with High Room-Temperature Figures of Merit. In *Materials for Sustainable Energy*; Co-Published with Macmillan Publishers Ltd, UK, 2010; pp 120–125. https://doi.org/10.1142/9789814317665_0019.

(15) Leblanc, S.; Yee, S. K.; Scullin, M. L.; Dames, C.; Goodson, K. E. Material and Manufacturing Cost Considerations for Thermoelectrics. *Renew. Sustain. Energy Rev.* **2014**, *32*, 313–327. https://doi.org/10.1016/j.rser.2013.12.030.

(16) Yee, S. K.; LeBlanc, S.; Goodson, K. E.; Dames, C. $ per W Metrics for Thermoelectric Power Generation: Beyond ZT. *Energy Environ. Sci.* **2013**, *6* (9), 2561–2571. https://doi.org/10.1039/C3EE41504J.

(17) Hu, Z.; Gao, S. Upper Crustal Abundances of Trace Elements: A Revision and Update. *Chem. Geol.* **2008**, *253* (3–4), 205–221. https://doi.org/10.1016/j.chemgeo.2008.05.010.

(18) Chen, B.; Uher, C.; Iordanidis, L.; Kanatzidis, M. G. Transport Properties of Bi 2 S 3 and

the Ternary Bismuth Sulfides KBi 6.33 S 10 and K 2 Bi 8 S 13. *Chem. Mater.* **1997**, *9* (7), 1655–1658. https://doi.org/10.1021/cm970033m.

(19) Mizoguchi, H.; Hosono, H.; Ueda, N.; Kawazoe, H. Preparation and Electrical Properties of Bi2S3 Whiskers. *J. Appl. Phys.* **1995**, *78* (2), 1376–1378. https://doi.org/10.1063/1.360315.

(20) Zhao, L.-D.; Zhang, B.-P.; Liu, W.-S.; Zhang, H.-L.; Li, J.-F. Enhanced Thermoelectric Properties of Bismuth Sulfide Polycrystals Prepared by Mechanical Alloying and Spark Plasma Sintering. *J. Solid State Chem.* **2008**, *181* (12), 3278–3282. https://doi.org/10.1016/j.jssc.2008.08.022.

(21) Yasin, S.; Hasko, D. G.; Ahmed, H. Fabrication of <5 Nm Width Lines in Poly(Methylmethacrylate) Resist Using a Water:Isopropyl Alcohol Developer and Ultrasonically-Assisted Development. *Appl. Phys. Lett.* **2001**, *78* (18), 2760–2762. https://doi.org/10.1063/1.1369615.

(22) Gangnaik, A. S.; Georgiev, Y. M.; Holmes, J. D. New Generation Electron Beam Resists: A Review. *Chem. Mater.* **2017**, *29* (5), 1898–1917. https://doi.org/10.1021/acs.chemmater.6b03483.

(23) Saifullah, M. S. M.; Subramanian, K. R. V.; Kang, D.-J.; Anderson, D.; Huck, W. T. S.; Jones, G. A. C.; Welland, M. E. Sub-10 Nm High-Aspect-Ratio Patterning of ZnO Using an Electron Beam. *Adv. Mater.* **2005**, *17* (14), 1757–1761. https://doi.org/10.1002/adma.200500484.

(24) Saifullah, M. S. M.; Asbahi, M.; Binti-Kamran Kiyani, M.; Tripathy, S.; Ong, E. A. H.; Ibn Saifullah, A.; Tan, H. R.; Dutta, T.; Ganesan, R.; Valiyaveettil, S.; Chong, K. S. L. Direct Patterning of Zinc Sulfide on a Sub-10 Nanometer Scale via Electron Beam Lithography.

ACS Nano **2017**, *11* (10), 9920–9929. https://doi.org/10.1021/acsnano.7b03951.

(25) Saifullah, M. S. M.; Asbahi, M.; Binti-Kamran Kiyani, M.; Liow, S. S.; Bin Dolmanan, S.; Yong, A. M.; Ong, E. A. H.; Ibn Saifullah, A.; Tan, H. R.; Dwivedi, N.; Dutta, T.; Ganesan, R.; Valiyaveettil, S.; Chong, K. S. L.; Tripathy, S. Room-Temperature Patterning of Nanoscale MoS2 under an Electron Beam. *ACS Appl. Mater. Interfaces* **2020**, *12* (14), 16772–16781. https://doi.org/10.1021/acsami.9b22229.

(26) Lundegaard, L. F.; Makovicky, E.; Boffa-Ballaran, T.; Balic-Zunic, T. Crystal Structure and Cation Lone Electron Pair Activity of Bi2S3 between 0 and 10 GPa. *Phys. Chem. Miner.* **2005**, *32* (8–9), 578–584. https://doi.org/10.1007/s00269-005-0033-2.

(27) Pala, N.; Karabiyik, M. Electron Beam Lithography (EBL). In *Encyclopedia of Nanotechnology*; Springer Netherlands: Dordrecht, 2016; pp 1033–1057. https://doi.org/10.1007/978-94-017-9780-1_344.

(28) Pradhan, N.; Katz, B.; Efrima, S. Synthesis of High-Quality Metal Sulfide Nanoparticles from Alkyl Xanthate Single Precursors in Alkylamine Solvents. *J. Phys. Chem. B* **2003**, *107* (50), 13843–13854. https://doi.org/10.1021/jp035795l.

(29) DePuy, C. H.; King, R. W. Pyrolytic Cis Eliminations. *Chem. Rev.* **1960**, *60* (5), 431–457. https://doi.org/10.1021/cr60207a001.

(30) Zhao, Y.; Chua, K. T. E.; Gan, C. K.; Zhang, J.; Peng, B.; Peng, Z.; Xiong, Q. Phonons in Bi2S3 Nanostructures: Raman Scattering and First-Principles Studies. *Phys. Rev. B* **2011**, *84* (20), 205330. https://doi.org/10.1103/PhysRevB.84.205330.

(31) Liu, Z.-Q.; Huang, W.-Y.; Zhang, Y.-M.; Tong, Y.-X. Facile Hydrothermal Synthesis of Bi2S3 Spheres and CuS/Bi2S3 Composites Nanostructures with Enhanced Visible-Light Photocatalytic Performances. *CrystEngComm* **2012**, *14* (23), 8261.

https://doi.org/10.1039/c2ce26123e.

(32) Panigrahi, P. K.; Pathak, A. The Growth of Bismuth Sulfide Nanorods from Spherical-Shaped Amorphous Precursor Particles under Hydrothermal Condition. *J. Nanoparticles* **2013**, *2013*, 1–11. https://doi.org/10.1155/2013/367812.

(33) Rath, T.; Padeste, C.; Vockenhuber, M.; Fradler, C.; Edler, M.; Reichmann, A.; Letofsky-Papst, I.; Hofer, F.; Ekinci, Y.; Griesser, T. Direct Extreme UV-Lithographic Conversion of Metal Xanthates into Nanostructured Metal Sulfide Layers for Hybrid Photovoltaics. *J. Mater. Chem. A* **2013**, *1* (37), 11135. https://doi.org/10.1039/c3ta12592k.

(34) Biswas, K.; Zhao, L.-D.; Kanatzidis, M. G. Tellurium-Free Thermoelectric: The Anisotropic n-Type Semiconductor Bi2S3. *Adv. Energy Mater.* **2012**, *2* (6), 634–638. https://doi.org/10.1002/aenm.201100775.

(35) Miura, A.; Mizuguchi, Y.; Takei, T.; Kumada, N.; Magome, E.; Moriyoshi, C.; Kuroiwa, Y.; Tadanaga, K. Structures and Optical Absorption of Bi2OS2 and LaOBiS2. *Solid State Commun.* **2016**, *227*, 19–22. https://doi.org/10.1016/j.ssc.2015.11.016.

(36) Huo, N.; Figueroba, A.; Yang, Y.; Christodoulou, S.; Stavrinadis, A.; Magén, C.; Konstantatos, G. Engineering Vacancies in Bi 2 S 3 Yielding Sub-Bandgap Photoresponse and Highly Sensitive Short-Wave Infrared Photodetectors. *Adv. Opt. Mater.* **2019**, *7* (11), 1900258. https://doi.org/10.1002/adom.201900258.

(37) Ramanery, F. P.; Mansur, A. A. P.; Mansur, H. S.; Carvalho, S. M.; Fonseca, M. C. Biocompatible Fluorescent Core-Shell Nanoconjugates Based on Chitosan/Bi2S3 Quantum Dots. *Nanoscale Res. Lett.* **2016**, *11* (1), 1–12. https://doi.org/10.1186/s11671-016-1417-6.

(38) Gulino, A.; Fragala, I. Deposition and Characterization of Transparent Thin Films of Zinc Oxide Doped with Bi and Sb. *Chem. Mater.* **2002**, *14* (1), 116–121.

https://doi.org/10.1021/cm011088y.

(39) Shi, X.; Wu, A.; Liu, W.; Moshwan, R.; Wang, Y.; Chen, Z.-G.; Zou, J. Polycrystalline SnSe with Extraordinary Thermoelectric Property via Nanoporous Design. *ACS Nano* **2018**, *12* (11), 11417–11425. https://doi.org/10.1021/acsnano.8b06387.

(40) Kumar, P.; Repaka, D. V. M.; Hippalgaonkar, K. Lithography-Free Resistance Thermometry Based Technique to Accurately Measure Seebeck Coefficient and Electrical Conductivity for Organic and Inorganic Thin Films. *Rev. Sci. Instrum.* **2017**, *88* (12), 125112. https://doi.org/10.1063/1.5012039.

(41) Lokhande, C. D.; Ubale, A. U.; Patil, P. S. Thickness Dependent Properties of Chemically Deposited Bi2S3 Thin Films. *Thin Solid Films* **1997**, *302* (1–2), 1–4. https://doi.org/10.1016/S0040-6090(96)09540-5.

(42) Mane, R. S.; Sankapal, B. R.; Lokhande, C. D. Studies on Chemically Deposited Nanocrystalline Bi2S3 Thin Films. *Mater. Res. Bull.* **2000**, *35* (4), 587–601. https://doi.org/10.1016/S0025-5408(00)00244-0.

(43) Chate, P. A.; Lakde, S. D. Electrical, Optical and Structural Properties of Rod Shaped Bi2S3 Thin Films Deposited by Dip Technique. *J. Mater. Sci. Mater. Electron.* **2015**, *26* (8), 5847–5851. https://doi.org/10.1007/s10854-015-3145-6.

(44) Ten Haaf, S.; Sträter, H.; Brüggemann, R.; Bauer, G. H.; Felser, C.; Jakob, G. Physical Vapor Deposition of Bi2S3 as Absorber Material in Thin Film Photovoltaics. *Thin Solid Films* **2013**, *535* (1), 394–397. https://doi.org/10.1016/j.tsf.2012.11.089.

(45) Recatala-Gomez, J.; Suwardi, A.; Nandhakumar, I.; Abutaha, A.; Hippalgaonkar, K. Toward Accelerated Thermoelectric Materials and Process Discovery. *ACS Appl. Energy Mater.* **2020**, acsaem.9b02222. https://doi.org/10.1021/acsaem.9b02222.

(46) Gorai, P.; Gao, D.; Ortiz, B.; Miller, S.; Barnett, S. A.; Mason, T.; Lv, Q.; Stevanović, V.; Toberer, E. S. TE Design Lab: A Virtual Laboratory for Thermoelectric Material Design. *Comput. Mater. Sci.* **2016**, *112*, 368–376. https://doi.org/10.1016/j.commatsci.2015.11.006.

(47) Danaei, R.; Varghese, T.; Ahmadzadeh, M.; McCloy, J.; Hollar, C.; Sadeq Saleh, M.; Park, J.; Zhang, Y.; Panat, R. Ultrafast Fabrication of Thermoelectric Films by Pulsed Light Sintering of Colloidal Nanoparticles on Flexible and Rigid Substrates. *Adv. Eng. Mater.* **2018**, *1800800*, 1–6. https://doi.org/10.1002/adem.201800800.

(48) Kalabukhov, A.; Gunnarsson, R.; Börjesson, J.; Olsson, E.; Claeson, T.; Winkler, D. Effect of Oxygen Vacancies in the SrTiO3 Substrate on the Electrical Properties of the LaAlO3/SrTiO3 Interface. *Phys. Rev. B* **2007**, *75* (12), 121404. https://doi.org/10.1103/PhysRevB.75.121404.

(49) Sarath Kumar, S. R.; Abutaha, A. I.; Hedhili, M. N.; Alshareef, H. N. Effect of Oxygen Vacancy Distribution on the Thermoelectric Properties of La-Doped SrTiO3 Epitaxial Thin Films. *J. Appl. Phys.* **2012**, *112* (11), 114104. https://doi.org/10.1063/1.4767840.

(50) Li, X.; Wang, Y.; Liu, W.; Jiang, G.; Zhu, C. Study of Oxygen Vacancies′ Influence on the Lattice Parameter in ZnO Thin Film. *Mater. Lett.* **2012**, *85*, 25–28. https://doi.org/10.1016/j.matlet.2012.06.107.

577

578 **TOC Figure**

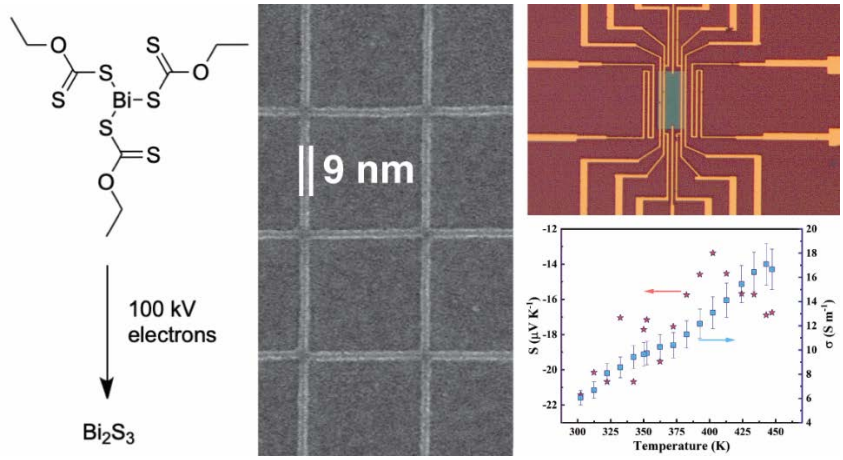

579